ACS APPLIED MATERIALS & INTERFACES

Research Article

www.acsami.org

One-Step Electrochemical Growth of a Three-Dimensional Sn–Ni@PEO Nanotube Array as a High Performance Lithium-Ion Battery Anode

Xin Fan,[†] Peng Dou,[†] Anni Jiang,[†] Daqian Ma,[†] and Xinhua Xu*[,†,‡]

[†]School of Materials Science and Engineering, Tianjin University, Tianjin 300072, P.R. China

[‡]Tianjin Key Laboratory of Composite and Functional Materials, Tianjin 300072, P.R. China

ABSTRACT: Various well-designed nanostructures have been proposed to optimize the electrode systems of lithium-ion batteries for problems like Li^+ diffusion, electron transport, and large volume changes so as to fulfill effective capacity utilization and increase electrode stability. Here, a novel three-dimensional (3D) hybrid Sn–Ni@PEO nanotube array is synthesized as a high performance anode for a lithium-ion battery through a simple one-step electrodeposition for the first time. Superior to the traditional stepwise synthesis processes of heterostructured nanomaterials, this one-step method is more suitable for practical applications. The electrode morphology is well preserved after repeated Li^+ insertion and extraction, indicating that the positive synergistic effect of the alloy nanotube array and 3D ultrathin PEO coating could authentically optimize the current volume-expansion electrode system. The electrochemistry results further confirm that the superiority of the Sn–Ni@PEO nanotube array electrode could largely boost durable high reversible capacities and superior rate performances compared to a Sn–Ni nanowire array. This proposed ternary hybrid structure is proven to be an ideal candidate for the development of high performance anodes for lithium-ion batteries.

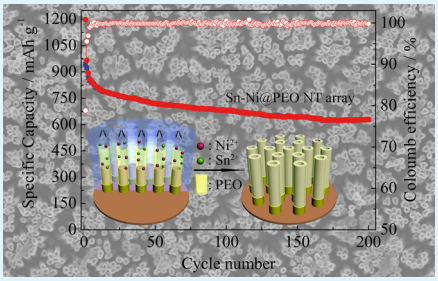

KEYWORDS: *tin-based anode, nanotube array, conformal coating, lithium-ion battery, electrochemical performance*

1. INTRODUCTION

Lithium-ion batteries have been widely used to power portable electronic devices because they possess the highest energy density among existing rechargeable batteries.[1−3] Tin-based anode materials have attracted extensive attention because of their high theoretical capacity of about 993 mA h g^{-1}.[4] Besides, their volumetric capacity (7254 mA h cm^{-3}) is about nine times as high as that of graphite (818 mA h cm^{-3}), which is highly favorable for portable lithium-ion battery applications.[5] However, the drastic volume change of an Sn-based electrode during repeated lithiation/delithiation would cause severe mechanical damage and lead to rapid capacity fading during cycling. Because the realization of high-performance lithium-ion batteries strongly relies on the electrical properties and mechanical integrity of the constitutive materials, the problems of structural stability caused by drastic volume change during cycling need prompt settlement.[6]

Accordingly, various strategies have been developed to optimize electrode structures or morphology.[6] First, the construction of novel structures such as highly porous and hollow nanostructures are extremely desirable with respect to their improvements in capacity utilization, charge-transport rate, and stable electrode structure on account of their large electrolyte/electrode contact area for lithium storage, short Li-ion diffusion distance in the solid phase, and rich pores as a good accommodation of volume expansion during the alloying process.[7−9] Furthermore, for the sake of maximizing mass loading of the active materials per geometric area without sluggish Li^+ intercalation and less-promising rate capability which are caused by the lack of enough active surface exposure,[10] 3D designs of electrode materials have been highly desirable since their open nanostructures associated with the high surface area as well as direct connection with the current collector would translate into high electrochemical capacities and good rate performance.[11] However, large surface area without protection would lead to more undesirable side reactions and continued capacity fading inevitably caused by the formation of a solid-electrolyte interphase (SEI) film, so surface modifications are needed to further ensure surface stability.[12]

Typically, one strategy to stabilize the surface and structure is to create core/shell nanostructures, which is expected to exploit the advantages of both components and offer special properties through a reinforcement or modification effect of each other.[13,14] The improvements generally include increasing the electronic conductivity, inhibiting structural changes during cycling, and reducing the thickness of the SEI film.[12] However, in consideration of the fact that the traditional synthesis processes of core–shell structure electrodes generally need at least two steps[14] and that achieving uniform coatings around nanostructured electrode materials has been challenging,[15] a facile synthesis route is highly needed.

Inspired by the issues mentioned above, we envision designing a sophisticated architecture composed of an Sn–Ni alloy nanotube array with an ultrathin conformal poly(ethylene oxide) (PEO) coating through a simple one-step electrodeposition process. The end-opened nanotube array with large surface-to-volume ratio is not only favorable for efficient ion transports but also capable of providing extra spaces to accommodate massive volume expansion during the alloying process. To the best of our knowledge, research about nanotube arrays for lithium-ion batteries is now concentrated on materials like Si,[16] TiO_2,[17] SnO_2,[18] and other binary metal oxides[19] which are deeply

Received: September 11, 2014
Accepted: November 25, 2014
Published: November 25, 2014

affected by poor electron transfer resulted from their semiconducting or even insulating property. In comparison, the Sn−Ni alloy nanotube array is more promising with its fine conductivity, high capacity, and the easy fabrication process. Ni is induced not only to enhance the mechanical strength and electron transfer dynamic along the 1D nanotube but also to partly alleviate the mechanical stress caused by the volume change of the Sn phase.[20] Meanwhile, ion-conductive polymer PEO is introduced not only to control the formation of SEI film and preserve the structural and interfacial stabilization of the electrode but also to contribute to the formation of hollow alloy nanotube structure possessing high Li^+/electron charge-transfer kinetics as well as excellent structural stability.[21] Thus, the judicious integration of ultrathin PEO conformal coating with Sn−Ni alloy nanotube array can effectively endow the electrodes with preferable cycling stability and rate capability. This Sn−Ni@PEO nanotube array prepared through a one-step electrodeposition can be considered as a promising candidate for a high performance lithium-ion battery anode.

2. EXPERIMENTAL SECTION

2.1. Preparation of the Sn−Ni@PEO Nanotube Array. In this fabrication process, the anodic alumina template (AAO, ANODISC 13) with an average pore diameter of 200 nm was purchased from WHATMAN. A conventional three-electrode cell is used, where an Ag/AgCl electrode immersed in the saturated KCl solution was used as the reference electrode, and a Pt foil was used as the counter-electrode. A film of gold was sputtered on one side of the alumina membrane as working electrode through ultra high vacuum magnetron sputtering coating machine (JGP-800). The gold layer is sputtered to ensure the conductive contact between AAO and Cu foil so that the Sn−Ni alloy could be deposited on to the Cu current collector in the pore of AAO template. After the first deposition layer of Sn−Ni alloy, the electron could be conducted through Sn−Ni conductive material itself, then nanowires or nanotubes could grow from bottom to top. The thickness of gold layer is about 90 nm. Then, the gold sputtered side of the AAO template was bonded to Cu using conductive silver adhesives. The electrolyte consisted of 17.82 g L^{-1} $NiCl_2{\cdot}6H_2O$, 39.4 g L^{-1} $SnCl_2{\cdot}2H_2O$, 165.15 g L^{-1} $K_4P_2O_7$, 9.38 g L^{-1} glycine, and 0.6 g L^{-1} PEO (M.W. 600 000). The galvanostatic electrodeposition of Sn−Ni@PEO nanotube array was performed on a PASTART2263 electrochemical workstation at a current density of 2 mA cm^{-2} for 2 h at room temperature. The Sn−Ni alloy was electrodeposited directly onto the Cu current. After that, the sample was immersed in 1 M NaOH solution to dissolve the AAO templates and was finally cleaned with deionized water (DI water). To validate the role of PEO during the development of the nanotube array architecture, a synthesis of the Sn−Ni nanowire array was attempted without PEO, while all other synthetic parameters remained identical to those for Sn−Ni@PEO nanotube array.

2.2. Characterization. The morphology and structure of the as-prepared samples were investigated by a Hitachi S-4800 field-emission scanning electron microscope (FE-SEM) at an accelerating voltage of 5 kV and a high-resolution transmission electron microscope (HR-TEM, JEM-2100F) operated at 200 kV. The composition of the electrode material was investigated using Genesis XM2 energy dispersive X-ray spectroscopy (EDS, USA). The crystal structure of the products were characterized by X-ray powder diffraction (XRD) using an automated D/MAX-2500 X-ray diffractmeter with monochromatic Cu Kα radiation, the 2 theta Bragg angles were scanned over a range of 25−85° at a rate of 5.0° min^{-1}. The Brunauer−Emmett−Teller (BET) specific surface area analysis was performed by measuring the N_2 adsorption−desorption isotherms at 77 K on a BelSorp-Mini instrument. The electrode materials after 200 cycles were washed with acetonitrile in the glovebox and than sealed in a hermetic bag before taken out to test.

2.3. Electrochemical Measurements. Electrochemical performance was investigated directly using coin cells (type CR2032) assembled in an argon-filled glovebox. Li metal foil was utilized as the counter electrode, 1 M $LiPF_6$ in ethylene carbonate (EC) and dimethyl carbonate (DMC) (1:1 by volume) was used as the electrolyte, the as-prepared Sn−Ni@PEO nanotube array electrode was used as the positive electrode, and Celgard 2400 was used as the separator. Each cell was aged for 24 h at room temperature before the electrochemical tests. The galvanostatic charge/discharge measurements and rate performance were performed over the potential range 0.01−2.0 V (vs Li^+/Li) using an LANHE battery testing system at room temperature. The electrochemical impedance spectroscopy (EIS, 0.1−1 × 10^6 Hz) was carried out by a CHI 660D system.

3. RESULTS AND DISCUSSION

The growth mechanism of the hybrid nanotube array, although not completely understood, is briefly suggested as follows. As presented in the schematic depiction for the synthesis of Sn−Ni@PEO nanotube array (Figure 1), the architecture is

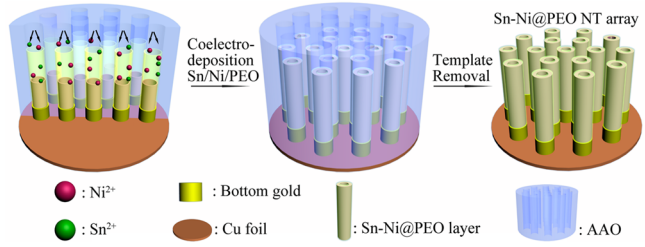

Figure 1. Schematic illustration for the formation of the Sn−Ni@PEO nanotube array.

obtained through a simple one-step electrodeposition in an aqueous electrolyte containing Ni^{2+}, Sn^{2+}, and PEO. Because the PEO molecule contains numerous polyether segments and terminal hydroxyl groups, it can not only physically form weak covalent bonds with the oxygen-containing functional groups on the surface of the AAO wall, but also attract Sn^{2+} and Ni^{2+} through electrostatic attraction.[22] Therefore, it is favorable for the fast electrochemical reduction along the pore wall. Meanwhile, PEO molecules adsorbed on the surface of the initial deposited Sn−Ni layer can produce an inhibition for further metal deposition perpendicular to the AAO walls. Thus, the function of PEO greatly contributes to the preferential growth of Sn−Ni alloy along the pore wall, realizing the formation of distinct heterostructure composed of Sn−Ni alloy nanotube array with conformal ultrathin PEO coating.

The detailed structure of Sn−Ni@PEO nanotube array and Sn−Ni nanowire array are schematically illustrated by FE-SEM. Top view images clearly show their upstanding tubular geometry (Figure 2a and c) and solid nanowire structure (Figure 2b and d), respectively. The dimensions of the two samples are identical (~200 nm). At low magnification in Figure 2a, all the nanotubes show well designed open end, which confirmed the ubiquity of the nanotube structure. Closer observation of the nanotube array depicted in Figure 2b reveals that the individual end-opened Sn−Ni@PEO nanotube has a

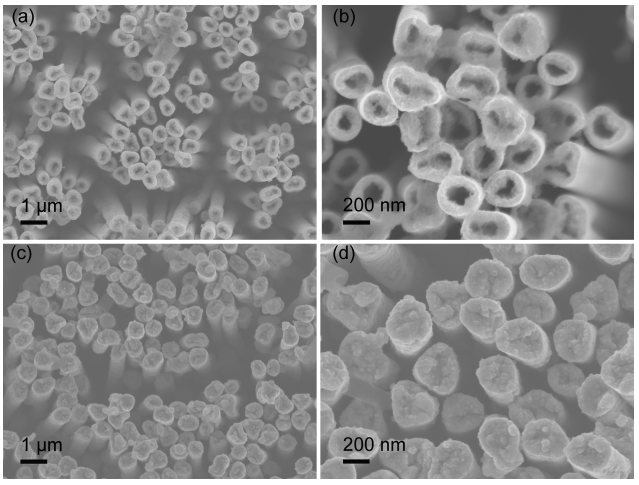

Figure 2. SEM images of (a and b) Sn−Ni@PEO nanotube array and (c and d) Sn−Ni nanowire array at different magnifications.

wall thickness of 50−60 nm with an inner diameter of ∼100 nm. Furthermore, the corresponding N_2 adsorption−desorption analysis shown in Figure 3 reveals that the end-opened

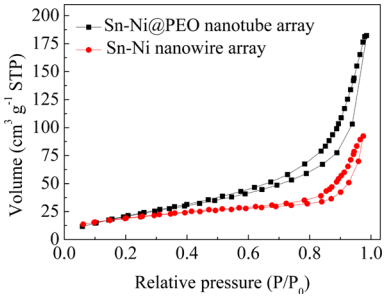

Figure 3. Surface areas of Sn−Ni@PEO nanotube array and Sn−Ni nanowire array.

Sn−Ni@PEO nanotube array possesses a large BET specific surface area of 87.6 m^2 g^{-1}, which is about one time higher than that of the Sn−Ni nanowire array (40.3 m^2 g^{-1}). With open ends and hollow interior, this electrode material can further reduce Li^+ diffusion length and achieve larger Li^+ flux at the active materials/electrolyte interface since the lithium insertion is available via both inner and outer surfaces. Significantly, in order to maximize the active sites for energy storage per geometric area and guarantee enough mass-loading for electrode materials to store a sufficient amount of energy, the lengths of the 1D nanotubes can be controlled by changing the deposition time. Though more severe agglomeration is unavoidable with longer nanotube arrays owing to their higher aspect ratio and lower stiffness, the ion-conductive PEO coating layer can serve as a geometrical separator to avoid the agglomeration effectively.[10] So this construction that combines the 3D open structure and flexible confining coating is expected to contribute to an upgraded cycling performance of anode materials.

Further insights into the morphology and structure of the resulting Sn−Ni@PEO nanotube arrays are carried out through TEM investigations. As shown in Figure 4a, the walls of the nanotube structure can be clearly identified as they appear to be darker under the TEM, while the hollow parts look brighter. The corresponding HR-TEM image taken at the edge of the

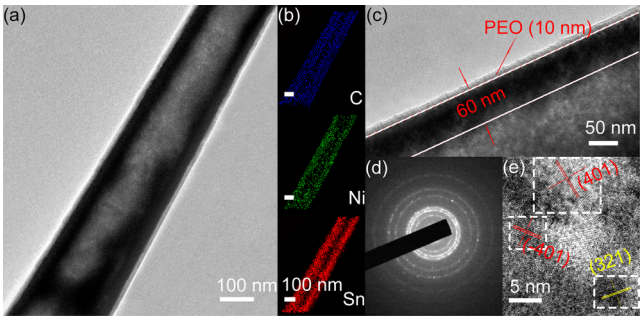

Figure 4. (a) TEM image of Sn−Ni@PEO nanotube and (b) corresponding elemental mapping of C, Ni, and Sn in Sn−Ni@PEO nanotube; (c) TEM image of detailed structure of the core/shell Sn−Ni@PEO nanotube at higher magnification (including the PEO layer and the inner alloy layer); (d) SAED patterns and (e) HR-TEM image of the Sn−Ni alloy layer.

core/shell nanotube clearly shows a well-developed electrode/polymer electrolyte interface and a uniform amorphous PEO coating layer with a thickness of ∼10 nm (Figure 4c). Meanwhile, a PEO coating layer forms on the inner wall of nanotube as well through the electrostatic attraction. This can be confirmed by EDS mapping as shown in Figure 4b that from the edge of inner wall of the nanotube to the outer wall, C has a wider distribution than Sn and Ni which are only observed up to 8−10 nm deep from the surface. This gives direct proof for the uniform surface modification of PEO on Sn−Ni nanotubes. The polycrystalline Sn−Ni alloy and low crystallized PEO are illustrated in the selected area electron diffraction (SAED) patterns from diffraction dots (Ni_3Sn_4) and weak rings (PEO) (Figure 4d). Moreover, the magnified lattice fringes of the inner alloy layer are shown in Figure 4e. There are two sets of overlapped lattices: the lattice indicated by the yellow arrow can be ascribed to the (321) facet of Sn (JCPDS 04-0673) whereas other lattices marked with red arrows match well with the (−401) and (401) planes of Ni_3Sn_4 (JCPDS 04-0845), respectively.

The molecular structures of the Sn−Ni@PEO composite were also characterized by FT-IR spectroscopy. The characteristic absorption of PEO in the samples are presented in Figure 5, which indicated that the main polymer chains of the Sn−Ni@PEO composite were similar to that of the PEO. It can be clearly seen that the characteristic peaks of PEO are located at around 3450, 2916, 2845, and 1168 cm^{-1}, which correspond to the stretching vibration of −OH, C−H, and C−O−C in the PEO chains, respectively. Besides, the characteristic peaks around 1436 cm^{-1} are related to the deformation vibrations of

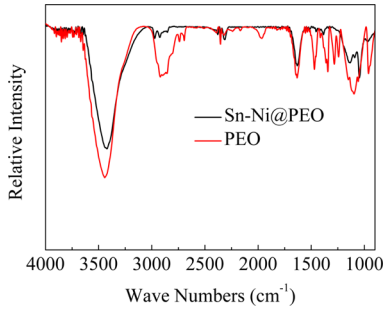

Figure 5. FT-IR spectra of Sn−Ni@PEO nanotube array and pure PEO.

dx.doi.org/10.1021/am506237y | ACS Appl. Mater. Interfaces 2014, 6, 22282−22288

C−H. The characteristic peaks around 1100 and 1350 cm^{-1} confirms the existence of crystal phase in PEO, which also implies that the degree of crystallinity in Sn−Ni@PEO composite is much less than that in pure PEO.

The crystallographic structure of Sn−Ni@PEO nanotube array is further analyzed by XRD as shown in Figure 6. Peaks of

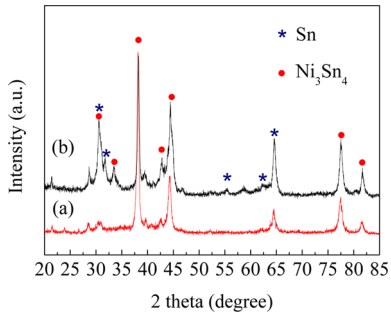

Figure 6. XRD profiles of (a) Sn−Ni nanowire array and (b) Sn−Ni@PEO nanotube array.

Ni_3Sn_4 alloy at around 30.9°, 33.4°, 38.6°, 43.9°, 44.6°, 78.3°, and 81.5° (JCPDS 04-0845) can be clearly identified, indicating that Ni_3Sn_4 is the predominant phase. Besides, when compared with the Sn−Ni nanowire array, the XRD pattern of Sn−Ni@PEO nanotube array shows stronger Sn peaks at 30.6°, 32.0°, 55.3°, 63.8°, and 64.6° (JCPDS 04-0673). This may be owing to the stronger inhibition effect of PEO on electrochemical reduction of Ni^{2+} than that of Sn^{2+}, thus hindering the formation of Sn−Ni alloys while relatively enhancing the formation pure Sn phase. As described in the EDS analysis, the atom ratio of Sn and Ni in Sn−Ni@PEO nanotubes is about 3:2 (Figure 7a), and in Sn−Ni nanowires, the atom ratio of Sn

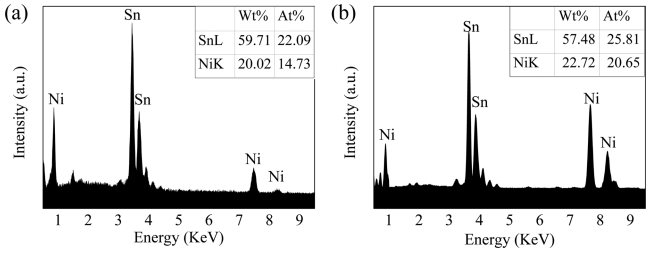

Figure 7. EDS microanalysis with corresponding element mass and atomic percentages of (a) Sn−Ni@PEO nanotube array and (b) Sn−Ni nanowire array.

and Ni is about 5:4, lower than the former (Figure 7b). The inactive phase in tin-based intermetallic compounds Ni_3Sn_4, Ni, can serve as a buffer which partly alleviates mechanical stress caused by the volume change of the active phase and act as a barrier against the aggregation of Sn during Li-ion insertion and extraction processes. It was found that higher capacity could be obtained when the electrode was a mixture of alloy and pure Sn.[23] Thus, as the Sn phase in the Sn−Ni@PEO nanotube array is much larger than that in the Sn−Ni alloy nanowire array, it can be expected that an Sn−Ni@PEO nanotube array anode can better enhance the capacity and cycle performance than the traditional Sn−Ni alloy anode.

The electrochemical cycling performance of the composite electrode is evaluated by galvanostatic charge/discharge cycling at a constant current density of 0.2 A g^{-1} from 2.0 to 0.01 V (Figure 8). For comparison, the Sn−Ni nanowire array

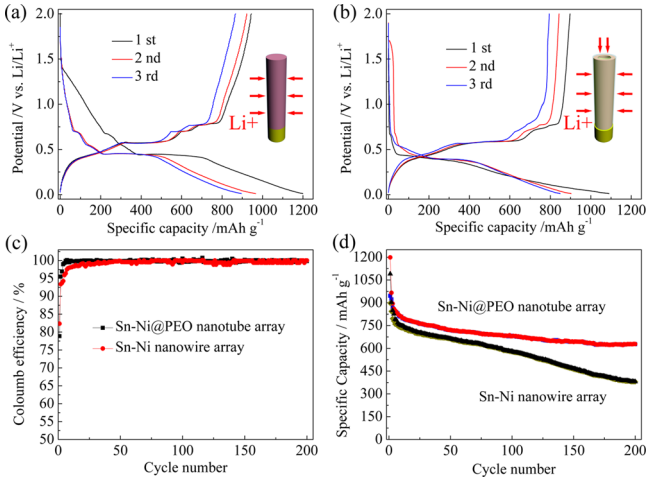

Figure 8. Galvanostatic charge/discharge curves of (a) Sn−Ni@PEO nanotube array (inset: schematic representation of solid nanowire configuration with the arrows indicating direction of Li ion transport); (b) Sn−Ni nanowire array for the initial three cycles (inset: schematic representation of the individual hollow nanotube morphology with the radial direction of Li ion transport); (c) Coulomb efficiency; and (d) cycle performance of Sn−Ni@PEO nanotube array and Sn−Ni nanowire array in the electrode potential range of 0.01−2.0 V (vs Li/Li^+) at 0.2 A g^{-1}.

electrode is also investigated under the same conditions. The voltage profiles of both samples show reversible electrochemical reactions at distinct voltage plateaus around 0.7, 0.54, and 0.456 V in discharge curves and 0.77, 0. 7, 0.57, and 0.45 V in charge curves, which are associated with the lithiation and delithiation processes of Li_xSn.[24] The electrochemical plateau above 0.75 V during the first cycle should be closely ascribed to the formation of SEI layer in the first cycle, which could not be avoided in the electrochemical cycling. The potential plateaus between 0.4 and 0.7 V can be mainly ascribed to Sn alloying with Li to form Li_xSn ($x < 2.33$), and the reactions below 0.3 V can be assigned to the further formation of Li_ySn ($3.5 < y < 4.4$) from Li_xSn ($x < 2.33$). For pure Sn, its reaction with lithium is a solid-solution (insertion) reaction. Lithium ions are added in the Sn phase. The reaction between Sn and lithium can be written generally as

$$Li + xSn \leftrightarrow LiSnx \quad (1)$$

For Sn−Ni alloy, its reaction with lithium is a displacement reaction.[25] When lithium reacts with Sn, the inactive Ni would be displaced or extruded from the parent phase. The extruded component Ni does not participate in the reactions but acts as a buffering matrix. The reaction between Ni_3Sn_4 and lithium can be written generally as

$$Li + xNi_ySn \rightarrow LiSn_x + xyNi \quad (2)$$

In other words, the actual reactions are the reactions between pure Sn phase and lithium. Because the Gibbs free-energy change for this reaction is the free energy of formation of product $LiSn_x$ subtracting the free energy required to cleavage x mole of compound $SnNi_y$. Consequently, the reaction equilibrium potential for compound $SnNi_y$ is lower than that for pure Sn phases.[25] Low charge−discharge polarization is obtained in both electrodes on account of the good electron conduction of the binder-free Sn−Ni alloy electrode. Moreover, as we can observe in Figure 8a and b, the voltage profile of Sn−Ni@PEO nanotube showed a little difference compared with

dx.doi.org/10.1021/am506237y | ACS Appl. Mater. Interfaces 2014, 6, 22282−22288

that of Sn−Ni nanowire electrodes; this can be caused by two factors. First, as shown in the XRD spectrum, the Sn−Ni@PEO nanotube has more Sn phase besides the Ni_3Sn_4 phase, so the multistep Li−Sn alloy reactions of Sn and Ni_3Sn_4 lead to a relatively smooth voltage profile of Sn−Ni@PEO nanotube. Second, because of the formation of hollow structure rely on the inhibition effect of PEO, the formed crystalline grain is smaller than that of solid Sn−Ni nanowire array and lead to increased surface area. Different surface and subsurface sites react at slightly different potentials, leading to a concomitant dispersion of values at which the electrochemical reaction takes place.[26] Specifically, the profiles of Sn−Ni@PEO nanotube array electrode show more stable plateaus than that of Sn−Ni nanowire array electrode, implying preferable reaction kinetics and cycling stability. The nanotube configuration shows an initial reversible capacity of ∼946 mA h g^{-1} whereas the nanowire configuration delivers an initial reversible capacity of ∼875 mA h g^{-1}. The difference in the initial capacity can be partly attributed to different accessibility of Li^+ to the active material. Li^+ transport in these configurations has been schematically illustrated in the respective plots in Figure 8a and b. It can be clearly seen that Sn−Ni nanotube array is endowed with shorter radial Li^+ diffusion distance and larger active material exposure. Though, for the Sn−Ni@PEO nanotube array, the large superficial area would consume more Li^+ during the formation of SEI film in the first cycle and lead to lower first coulomb efficiency (∼78.9%) as shown in Figure 8c, its average coulomb efficiency from the second to 200th cycle remains 99.8%, higher than that of the nanowire array. This strongly indicates the well maintained reversibility of electrochemical reactions on account of stable electrode structure and the effectively avoided detrimental reactions between Sn and electrolyte through the conformal coating of PEO. From Figure 8d, the Sn−Ni@PEO nanotube array electrode exhibits a high reversible capacity of 628 mA h g^{-1} over 200 cycles, corresponding to 63% capacity retention. This is more promising than that of Sn−Ni alloy nanowore array conducted by Yang et al.,[27] which showed a capacity of ∼470 mA h g^{-1} after 50 cycles, confirming that the synergistic effect of hollow structure with conformal coating would contribute to better electrochemical performance then solid structure electrode materials. In our research, the capacity of Sn−Ni nanowire array electrode fades to a value of 380.5 mA h g^{-1} after 200 cycles, corresponding to only 38% capacity retention. The cycle stability and reversible capacity of Sn−Ni@PEO nanotube array is markedly superior to that of Sn−Ni nanowire array.

This improved performance can be put down to the end-opened alloy nanotube structure which can not only provide larger materials/electrolyte interface for shorter Li^+ diffusion length and larger Li^+ flux at the interface but can also effectively accommodate the local volume change during Li insertion/desertion. The enhanced structure and surface stabilization is demonstrated through SEM investigations. As shown in Figure 9b, when fully lithiated in the first cycle, the thickness of the tube wall increases about 23 nm while total expansion of diameter only shows a modest increase of about 10 nm. The hollow interior largely absorbs the volume expansion. While the lithiated nanowire suffers a dramatic radial expansion of ∼20 nm, and the spaces between nanowires are completely occupied (Figure 9e). The drastic volume change would inherently result in severe pulverization of the electrode materials upon electrochemical cycling and lead to the formation of a thick

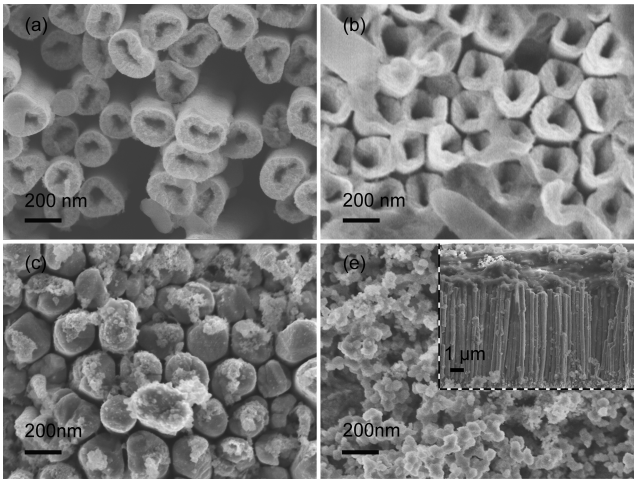

Figure 9. SEM images of the (a, b) Sn-Ni@PEO nanotube array and (c, d) Sn-Ni@PEO nanotube array electrode (a, c) after first lithiation, and (b, e) full delithiation after 50 cycles.

SEI films which would cause the consumption of more Li^+ and a large irreversible capacity. After complete delithiation after 50 cycles, the structure integrality of the nanotube array is well preserved without obvious SEI formation (Figure 9b), wall thickness expanded a little, which is caused by the Li trapped in the anode materials during cycling. Meanwhile, there still exist enough spaces between adjacent nanotubes as we can see from the top view. Despite the fact that the smooth wall surface becomes rough due to the repeated lithiation/delithiation reactions, the integral structure remains almost the same with the pristine product, confirming the durable electrode integrity in long-term operation. In addition, a thick SEI film covered the surface of the nanowire array as we can see in Figure 9d, the SEI film mainly covered above the array, while the inner nanowires remained the same. Because of the serious formation of SEI film and lack of channels for electrolyte permeation, the active materials cannot be fully used and the reverse capacity drops rapidly.

Apart from the well designed structure that enhanced the electrode stability, the interfacial stabilization effect of conformal PEO coating is also important. The SEI formation on Sn-based anode appears to be a dynamic process of breaking off and reforming due to the new surfaces exposure to electrolyte caused by the constant volume change during cycling, which would cause a large amount of Li^+ and sacrifice the reversible capacity. Therefore, the SEI stability on the negative electrode is critical to the cycling characteristics of electrodes, especially for electrode materials suffering from severe volume expansion. Coating with soft PEO film on the surface of Sn−Ni alloy can not only prevent the direct contact of active materials with the electrolyte but also accommodate the internal stress of anodes suffering from severe volume change, thus ensuring the stability of the SEI film and reduce of the thickness of the SEI layer. According to the BET analysis taken after 50 cycles, the large surface area of the 3D end-opened nanotube array is better maintained than that of the solid nanowire array (Figure 10), indicating that stable electrode/electrolyte contact and fast lithiation/delithiation kinetics are allowed throughout the cycling test of Sn−Ni@PEO nanotube array electrode. Yet on the other hand, the deteriorated cycling performances of nanowire array electrode can also be ascribed to the agglomeration of solid nanowires

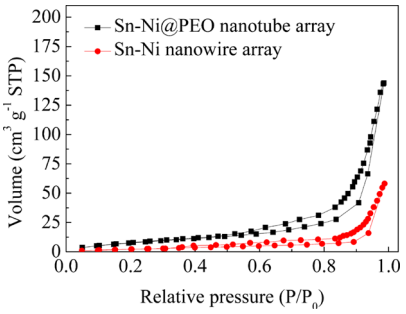

Figure 10. Surface areas of Sn−Ni@PEO nanotube array and Sn−Ni nanowire array after 50 cycles.

and the formation of thick SEI film which largely blocks the Li^+ transportation and causes inadequate utilization of inner active materials.

To evaluate the merits of this hybrid nanotube array architecture for fast electrochemical reaction kinetics, the rate performances are tasted at variable current densities. As shown in Figure 11a, the charge/discharge curves of Sn−Ni@PEO

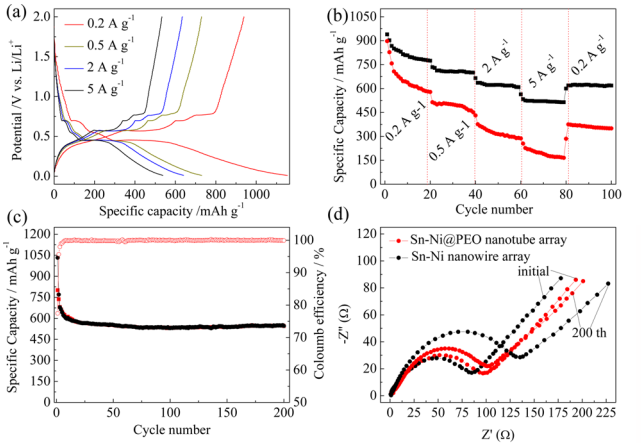

Figure 11. (a) Charge/discharge profiles of Sn−Ni@PEO nanotube array electrode at various current densities; (b) rate performance demonstration of Sn−Ni@PEO nanotube array (black) and Sn−Ni nanowire array electrodes (red) at different current densities; (c) lithiation/delithiation capacities and coulomb efficiency of Sn−Ni@PEO nanotube array electrode cycled at 5.0 A g^{-1} for 200 cycles; (d) typical Nyquist plots of the Sn−Ni@PEO nanotube array and Sn−Ni nanowire array electrodes after the first and 200 cycles respectively at the fully delithiation state (1.5 V vs Li^+/Li). 1 C is equal to 993 mA h g^{-1}.

nanotube array electrode at different current densities show evident plateaus without obvious differences. When the charge/discharge current increased to 5 A g^{-1}, the lithiation/delithiation potential still shows a step profile, indicating highly reversible Sn−Li alloy/dealloy reactions at higher charge/discharge rates. According to Figure 11b, reversible capacities of the Sn−Ni@PEO nanotube array electrode are 939, 729, 635, and 533 mA h g^{-1} at the increasing current densities of 0.2, 0.5, 2, and 5 A g^{-1} every 20 cycles, respectively. When the current density is switched back to the initial 0.2 A g^{-1} after 80 cycles, the composite electrode retains its capacity of about 619 mA h g^{-1}, while the capacities of the Sn−Ni nanowire array electrode decrease rapidly to a capacity of about 170 mA h g^{-1} at a current density of 5 A g^{-1} after 80 cycles. To fully illustrate the rapid transport capabilities of the Sn−Ni@PEO nanotube array anode, the deep cycling results at higher rate are shown in Figure 11c. A stabilized capacity of 545 mA h g^{-1} is achieved with high coulomb efficiency at a current density of 5 A g^{-1} after 200 cycles.

In essence, the high rate capability and the cycle stability are tightly related to the thickness of SEI film, interfacial charge-transfer process, and Li^+ diffusion in the composite. To gain further insight into the advantages of Sn−Ni@PEO nanotube array anode, EIS measurements are carried out after the first and 200th cycle respectively at the fully delithiation state (1.5 V vs Li^+/Li). The complex plane plots for each sample can be divided into high frequency semicircle and low frequency sloping line (Figure 11d). The high frequency intercept of the semicircle is generally considered as electrical conductivity of electrodes, electrolyte, and separator, and it remained almost constant after 200 cycles for both electrodes. The depressed semicircle in the high-frequency range is correlated to the resistance of the SEI layer formed on the surface of electrode (R_{sf}) and the charge-transfer resistance (R_{ct}) between the surface films and the active material. After 200 cycles, no obvious $R_{(sf+ct)}$ impedance increase is detected for Sn−Ni@PEO nanotubes array after 200 cycles, indicating the stable thin SEI layer and quick lithium-ion diffusion rate. Meanwhile, the impedance for Sn−Ni nanowire array increases significantly after cycling. This could be attributed to the stable structure of Sn−Ni@PEO nanotubes array which could effectively ease the pile-up of SEI during cycling process, and the specific hollow nanotube structure can increase the exchange rate of electrode material and electrolyte ions. Furthermore, in the low frequency area, the phase angle for impedance plot of the Sn−Ni@PEO nanotube array is much higher than that of the Sn−Ni nanowire array after 200 cycles, indicating a faster Li^+ diffusion in the nanotube structure during repeated charge/discharge processes.

Hence, the good cycling and rate performance of hybrid nanotube array electrode can be attributed to the synergetic effect of four factors: first is the high utilization of electrode materials and fast Li^+ transport dynamic on account of large active materials' exposure and short ion diffusion lengths; second is the enhancement of the electronic conductivity along the one-dimensional nanotube structure through the introduction of Ni and the direct connection with the current collector; third is the well-defined hollow nanotube structure which is capable of buffering the huge volume expansion and provide larger materials/electrolyte interface for faster reaction kinetics; fourth is the combination of the merits of intermetallic compounds and high capacity of Sn; the last but very important factor is the ultrathin PEO coating which not only contributes to the formation of hollow structures but also helps stabilize the SEI film while maintaining excellent ionic conductivity and provides elastic accommodation to restrain substantial electrode agglomeration and pulverization.

4. CONCLUSIONS

In conclusion, a facile route has been developed to directly grow a Sn−Ni@PEO nanotube array through a one-step electrodeposition. In this well engineered ternary hybrid architecture, the desired structural features of each component are thoroughly presented to guarantee sufficient exposure of active sites, highways for ion/electron transport, and excellent structural/interfacial stability. The electrode morphology is well preserved after repeated Li^+ insertion and extraction, and the electrochemistry results confirm that all the features of this

novel anode material are simultaneously and authentically in favor of optimizing the current volume-expansion electrode system of the lithium-ion battery to achieve full utilization of the active materials and stable cycling performance with long life-span at high rates. Besides, superior to the traditional stepwise synthesis processes of core−shell structure, the well-designed alloy nanotybe array with uniform PEO coating achieved in the one-step process is more suitable for practical applications, and this proposed ternary hybrid structure is an ideal candidate for the development of high performance anode materials of lithium-ion batteries.

AUTHOR INFORMATION

Corresponding Author

*E-mail address: xhxu_tju@eyou.com.

Notes

The authors declare no competing financial interest.

ACKNOWLEDGMENTS

This work was financially supported by the National Natural Science Foundation of China (Nos. 51143009 and 51273145).

REFERENCES

(1) Armand, M.; Tarascon, J. M. Building Better batteries. *Nature* **2008**, *451*, 652−657.
(2) Kang, K.; Meng, Y. S.; Breger, J.; Grey, C. P.; Ceder, G. Electrodes with High Power and High Capacity for Rechargeable Lithium Batteries. *Science* **2006**, *311*, 977−980.
(3) Kang, B.; Ceder, G. Battery Materials for ultrafast Charging and Discharging. *Nature* **2009**, *458*, 190−193.
(4) Winter, M.; Besenhard, J. O. Electrochemical Lithiation of Tin and Tin-based Intermetallics and Composites. *Electrochim. Acta* **1999**, *45*, 31−50.
(5) Qin, J.; He, C. N.; Zhao, N. Q.; Wang, Z. Y.; Shi, C. S.; Liu, E. Z.; Li, J. J. Graphene Networks Anchored with Sn@Graphene as Lithium Ion Battery Anode. *ACS Nano* **2014**, *8*, 1728−1738.
(6) Mukherjee, R.; Krishnan, R.; Lu, T. M.; Koratkar, N. Nanostructured Electrodes for High-power Lithium Ion Batteries. *Nano Energy* **2012**, *1*, 518−533.
(7) Yu, F.; Ge, S. G.; Li, B.; Sun, G. Z.; Mei, R. G.; Zheng, L. X. Three-Dimensional Porous $LiFePO_4$: Design, Architectures and High Performance for Lithium Ion Batteries. *Curr. Iorg. Chem.* **2012**, *2*, 194−212.
(8) Ge, M. Y.; Lu, Y. H.; Ercius, P.; Rong, J. P.; Fang, X.; Mecklenburg, M.; Zhou, C. W. Large-Scale Fabrication, 3D Tomography, and Lithium-Ion Battery Application of Porous Silicon. *Nano Lett.* **2014**, *14*, 261−268.
(9) Chen, X. L.; Guo, J. C.; Gerasopoulos, K.; Langrock, A.; Brown, A.; Ghodssi, R.; Culver, J. N.; Wang, C. S. 3D Tin Anodes Prepared by Electrodeposition on a Virus Scaffold. *J. Power Sources* **2012**, *211*, 129−132.
(10) Zhu, J. X.; Yang, D.; Rui, X. H.; Sim, D. H.; Yu, H.; Hoster, H. E.; Ajayan, P. M.; Yan, Q. Y. Facile Preparation of Ordered Porous Graphene-Metal Oxide@C Binder-Free Electrodes with High Li Storage Performance. *Small* **2013**, *9*, 3390−3397.
(11) Liu, R.; Duay, J.; Lee, S. B. Heterogeneous Nanostructured Electrode Materials for Electrochemical Energy Storage. *Chem. Commun.* **2011**, *47*, 1384−1404.
(12) Fu, L. J.; Liu, H.; Li, C.; Wu, Y. P.; Rahm, E.; Holze, R.; Wu, H. Q. Surface Modifications of Electrode Materials for Lithium Ion Batteries. *Solid State Sci.* **2006**, *8*, 113−128.
(13) Xia, X. H.; Tu, J. P.; Zhang, Y. Q.; Wang, X. L.; Gu, C. D.; Zhao, X. B.; Fan, H. J. High-Quality Metal Oxide Core/Shell Nanowire Arrays on Conductive Substrates for Electrochemical Energy Storage. *ACS Nano* **2012**, *6*, 5531−5538.
(14) Mai, L. Q.; Dong, F.; Xu, X.; Luo, Y. Z.; An, Q. Y.; Zhao, Y. L.; Pan, J.; Yang, J. G. Cucumber-Like V_2O_5/poly(3,4-ethylenedioxythiophene)&MnO_2 Nanowires with Enhanced Electrochemical Cyclability. *Nano Lett.* **2013**, *13*, 740−745.
(15) Gowda, S. R.; Reddy, A. L. M.; Shaijumon, M. M.; Zhan, X. B.; Ci, L. J.; Ajayan, P. M. Conformal Coating of Thin Polymer Electrolyte Layer on Nanostructured Electrode Materials for Three-Dimensional Battery Applications. *Nano Lett.* **2011**, *11*, 101−106.
(16) Ha, J.; Paik, U. Hydrogen Treated, End-opened Si Nanotubes Array Anode for High Power Lithium Ion Battery. *J. Power Sources* **2013**, *244*, 463−468.
(17) Guo, W. X.; Xue, X. Y.; Wang, S. H.; Lin, C. J.; Wang, Z. L. An Integrated Power Pack of Dye-Sensitized Solar Cell and Li Battery Based on Double-Sided TiO_2 Nanotube Arrays. *Nano Lett.* **2012**, *12*, 2520−2523.
(18) Wang, Y.; Lee, J. Y.; Zeng, H. C. Polycrystalline SnO_2 Nanotubes Prepared via Infiltration Casting of Nanocrystallites and Their Electrochemical Application. *Chem. Mater.* **2005**, *17*, 3899−3903.
(19) Wang, Z. Y.; Zhou, L.; Lou, X. W. Metal Oxide Hollow Nanostructures for Lithium-ion Batteries. *Adv. Mater.* **2012**, *24*, 1903−1911.
(20) Hassoun, J.; Panero, S.; Simon, P.; Taberna, P. L.; Scrosati, B. High-Rate, Long-Life Ni-Sn Nanostructured Electrodes for Lithium-Ion Batteries. *Adv. Mater.* **2007**, *19*, 1632−1635.
(21) Gowda, S. R.; Reddy, A. L. M.; Zhan, X. B.; Ajayan, P. M. Building Energy Storage Device on a Single Nanowire. *Nano Lett.* **2011**, *11*, 3329−3333.
(22) Wang, J.; Ran, R.; Tade, M. O.; Shao, Z. P. Self-assembled Mesoporous TiO_2/carbon Nanotube Composite with a Three-dimensional Conducting Nanonetwork as a High-rate Anode Material for Lithium-ion Battery. *J. Power Sources* **2014**, *254*, 18−28.
(23) Tamura, N.; Kato, Y.; Mikami, A.; Kamino, M.; Matsuta, S.; Fujitani, S. Study on Sn-Co Alloy Electrodes for Lithium Secondary Batteries. *J. Electrochem. Soc.* **2006**, *153*, A2227−A2231.
(24) Jiang, D. D.; Ma, X. H.; Fu, Y. B. High-performance Sn-Ni Alloy Nanorod Electrodes Prepared by Electrodeposition for Lithium Ion Rechargeable Batteries. *J. Appl. Electrochem.* **2012**, *42*, 555−559.
(25) Zhang, W. J. Lithium insertion/extraction mechanism in alloy anodes for lithium-ion batteries. *J. Power Sources* **2011**, *196*, 877−885.
(26) Xu, L. P.; Kim, C. J.; Shukla, A. K.; Dong, A. G.; Mattox, T. M.; Milliron, D. J.; Cabana, J. Monodisperse Sn Nanocrystals as a Platform for the Study of Mechanical Damage during Electrochemical Reactions with Li. *Nano Lett.* **2013**, *13*, 1800−1805.
(27) Tian, M.; Wang, W.; Yang, R. G. Stable High Areal Capacity Lithium-ion Battery Anodes Based on Three-dimensional Ni-Sn Nanowire Networks. *J. Power Sources* **2012**, *211*, 46−51.